

Learning to find order in disorder

Humberto Munoz-Bauza,¹ Firas Hamze,² and Helmut G. Katzgraber^{3,4,5}

¹*Department of Physics and Astronomy, University of Southern California, Los Angeles, California 90089, USA*

²*D-Wave Systems, Inc. 3033 Beta Avenue, Burnaby, British Columbia, V5G 4M9, Canada*

³*Microsoft Quantum, Microsoft, Redmond, WA 98052, USA*

⁴*Department of Physics and Astronomy, Texas A&M University, College Station, Texas 77843-4242, USA*

⁵*Santa Fe Institute, 1399 Hyde Park Road, Santa Fe, New Mexico 87501 USA*

We introduce the use of neural networks as classifiers on classical disordered systems with no spatial ordering. In this study, we implement a convolutional neural network trained to identify the spin-glass state in the three-dimensional Edwards-Anderson Ising spin-glass model from an input of Monte Carlo sampled configurations at a given temperature. The neural network is designed to be flexible with the input size and can accurately perform inference over a small sample of the instances in the test set. Using the neural network to classify instances of the three-dimensional Edwards-Anderson Ising spin-glass in a (random) field we show that the inferred phase boundary is consistent with the absence of an Almeida-Thouless line.

I. INTRODUCTION

Machine learning methods are a class of artificial intelligence algorithms that learn to perform tasks through the extraction of patterns from data sets. Artificial neural networks, or simply neural networks (NN), are machine learning methods inspired by biological neural systems and are suitable for function approximation, image classification, and various other pattern recognition tasks [1–3]. Recently, machine learning methods, and neural networks in particular, have also found applications in computational condensed matter physics with phase transition detection in both classical and quantum systems [4, 5]. A potential advantage of neural networks is their ability to generalize their learning when applied to a different—but closely related—class of data. For instance, Ref. [5] used a convolutional neural network trained on the Fermi-Hubbard model of correlated electrons at half-filled chemical potential to infer the transition temperature away from half filling, where the Hamiltonian suffers from the “sign problem” of quantum Monte Carlo. This suggests that machine learning can provide insight in situations where Monte Carlo methods may not be readily available or might require exorbitant numerical effort.

Here we introduce the use of phase classifying machine learning methods for spin glasses [6–9], archetypal disordered frustrated magnets for which there is little theoretical understanding when the models are short ranged and where numerical simulations are typically extremely difficult, thus requiring vast amounts of CPU time. Possibly the most controversial aspect in the theory of spin glasses is the existence of a spin-glass state in the presence of a field. While the replica-symmetry breaking picture of Parisi [10] predicts a spin-glass state for short-range systems, the “droplet picture” of Fisher and Huse [11–14] states that any infinitesimal (random) field destabilizes the spin-glass state at all finite temperatures. There have been numerous attempts to numerically establish the existence of a spin-glass state in a field for short-range systems with contradicting results. While some [15–22] find

no evidence of a transition, other studies seem to detect a spin-glass state in a field [23–27], i.e., the de Almeida-Thouless line [28]. In particular, there has been disagreement on the different observables to be used [21, 24], especially given the strong finite-size effects typically observed in spin-glass simulations. We note that the possibility of a critical dimension above which a spin-glass state occurs for a short-range system in a field has also been considered [29].

To demonstrate the potential utility of machine learning and work around the issues imposed by different observables typically measured in spin-glass simulations, here we use a neural network to search for a stable spin-glass phase in the presence of a (random) field in the three-dimensional Edwards-Anderson Ising spin glass and compare to results of Ref. [17].

We implement a neural network architecture using the TensorFlow [30] library for Python and find that it demonstrates strong evidence of learning a representation of the three-dimensional spin-glass state at zero field, if also given the opportunity to learn from simple three-dimensional ferromagnetic data to additionally distinguish a ferromagnetic state. The main advantages of our implementation are as follows. First, the approach makes classification inferences on the basis of multiple instance samples of the spin-glass Hamiltonian and multiple configuration samples from each instance. Second, its input can consist of configurations of any linear system size $L \geq 6$ by assuming periodic boundary conditions. We test the ability of the NN to generalize its knowledge when the spin-glass Hamiltonian has a nonzero field and find the classification results to be consistent with the Monte Carlo results of Ref. [17], i.e., that a spin-glass state is not stable in an external field for a three-dimensional short-range system.

The paper is structured as follows. In Sec. II we introduce the model we study, followed by details of our NN implementation and simulation details. Results are presented in Sec. III, followed by concluding remarks.

II. MODEL, COMPUTATIONAL METHODS AND NEURAL NETWORKS

A. Model

The Edwards-Anderson Ising spin glass model [31] is described by the Hamiltonian

$$H = - \sum_{\langle ij \rangle} J_{ij} s_i s_j - \sum_i h_i s_i, \quad (1)$$

where each J_{ij} and h_i is a random variable drawn from a given symmetric probability distributions. In zero-field models, $h_i = 0 \forall i$. In this paper we primarily consider the couplings J_{ij} to be drawn from a Gaussian distribution of unit variance. In nonzero field models, each field h_i is drawn from a Gaussian distribution standard deviation h .

B. Motivating the design of our neural network

Carrasquilla and Melko [4] implemented a multi-layer perceptron (MLP)—a neural network with a single hidden layer—to distinguish the ferromagnetic and paramagnetic states on the two-dimensional Ising model and detecting its phase transition regime by finding the point where the classification probabilities cross. Using arrays of spin configurations sampled from Monte Carlo simulations as inputs, their neural network was trained to classify single configuration samples as being in a ferromagnetic or paramagnetic state. With the resulting classification probabilities, one can identify a transition temperature T_c from where the probabilities cross. The neural network successfully discriminates between the ferromagnetic (FM) and paramagnetic (PM) phases for linear system sizes between $L = 10$ and $L = 60$, with a natural classification error occurring in the vicinity of the phase transition temperature $T_c \approx 2.269$ [32]. They find that the representation of the ferromagnetic phase in the MLP is tied to learning the average magnetization m by comparing it with a toy-model MLP in which the hidden layer is simplified to directly measure m , while leaving a single free parameter that is learned during training.

Following the initial results of Ref. [4], Ch’ng *et al.* [5] implemented a three-dimensional convolutional neural network (CNN) to distinguish the Néel transition in the three-dimensional Fermi-Hubbard model at half-filling, and extrapolated its magnetic phase diagram as the chemical potential is varied, which is problematic to study as the sign problem of quantum Monte Carlo becomes significant. This paper has the analogous objective of identifying the spin-glass state in the Edwards-Anderson model and establishing its phase boundary, with the benefit that past Monte Carlo studies are available to compare with.

An outline of the motivations for the neural network design is as follows:

1. The spin configuration snapshots of the spin-glass model at low temperatures are visually indistinguishable from paramagnetic ones. To overcome this problem, as inputs for learning we use replica overlap configurations

$$q_i = s_i^{(1)} s_i^{(2)} \quad (2)$$

taken from two independent Markov chains (1) and (2). The usual overlap parameter q [6] is the sum of the q_i with $i \in \{1, \dots, N\}$ and $N = L^3$ the number of spins.

2. The networks in Ref. [4] infer a phase using a single Monte Carlo configuration sample at a time as the input to the neural network. To ensure reliable phase classification, we implement a CNN that averages over multiple configuration samples from a Monte Carlo simulation.
3. To learn a reasonable representation for the spin-glass state, a neural network should consider configurations across multiple instances simulated at the same temperature T and with the same field strength h , as the critical properties for a spin-glass transition are considered from a quenched average. Thus, we propose that an averaging step over a sample of instances (instance averaging) is necessary for a NN to classify the spin-glass state faithfully.
4. It is possible that a supervised binary classifier for the spin glass (SG) and PM phases may learn to represent the SG state in a way that is only sensitive to the magnitude of the overlap parameter q . While such a classifier would probably be successful in a zero-field model, one could question whether such a classifier has truly “learned” the spin-glass state. However, teaching a classifier to also distinguish between the SG and FM phases helps create a better knowledge representation of the SG state that is not too directly tied to $|q|$. For both a typical spin-glass replica and for the Ising ferromagnet, there is a large probability of $q \approx \pm 1$ below the critical point. However, intermediate values of q between -1 and 1 are likely only in a spin-glass model due to nontrivial ergodicity breaking. Thus, this motivates a design for a phase classifier that is taught *three categories*, i.e., a ternary classifier, of the FM, PM, and SG states.
5. When generalizing to the nonzero field case, the mean of each q_i is biased because the spins become more likely to point in the direction of their local field. Thus, each q_i should be centered around its thermal mean $\langle q_i \rangle$.

C. Convolutional neural network and training

The ternary state classifying neural network (hereafter referred to as the *classifier*) is a three-dimensional convolutional neural network with two convolutional layers that extract spatial information from the overlap samples from each instance, followed by two fully-connected layers with intermediate averaging steps. The classifier is detailed in Algorithm 1. The predictions of the CNN for a single example manifest in line 10 as a vector y_i of three real numbers, which are not necessarily bounded. The last step applies the “softmax” function to create probabilities

$$p_i = \frac{e^{y_i}}{\sum_j e^{y_j}} \quad (3)$$

that can be interpreted as the degree of belief that a given example belongs to in each class (state) i . We refer to these probabilities as *softmax probabilities*. However, the results presented here utilize a *classification probability* of a category i , which is the rate that i is the most likely class (largest p_i) for the instances at a given temperature. This is the more practical measure for testing a NN.

During training we wish to align the prediction of the CNN as close as possible to the actual label of the example by adjusting the parameters of each layer of the CNN. In other words, we would like to match the softmax probabilities p_i as close as possible with the indicator probabilities d_i , where $d_i = 1$ if i is the index of the correct state, and 0 otherwise. This can be cast as a numerical optimization problem of a cost function $C(p_i, d_i)$. Here, the cost function is the negative cross entropy of the probabilities,

$$C(p_i, d_i) = - \sum_i [d_i \ln p_i + (1 - d_i) \ln(1 - p_i)]. \quad (4)$$

The general strategy in machine learning is to calculate the numerical gradient of the cost function for a batch of examples and adjust the NN parameters in the negative gradient direction until a minimum for C is reached. The simplest gradient strategy is called stochastic gradient descent (SGD). However, in this paper we use the ADAM [33] method, an adaptive variant of SGD, for training the parameters of the neural network along with an ℓ^2 penalty on the cost function. Further details on NN training can be found, for example, in Refs. [1] and [2].

In Algorithm 1, the hyperparameters B , Q , and R specify the grouping sizes of the training examples for every training step. B is the number of examples in each step (the batch size), Q is the number of spin-glass instances randomly selected in each example, and R is number of overlap configuration samples for each instance. Per the second and third motivations in Sec. II B, a single example is a 2-tensor of three-dimensional configurations, with dimensions $Q \times R \times L^3$, which is progressively reduced through the layers of the CNN into the vector p_i of

Algorithm 1 Convolutional neural network design for state classification on cubic lattices

- 1: **procedure** SG-NET-EVAL (Constants: B batch size, Q instances per example, R overlap samples per instance; Input: $B \times Q \times R \times L^3$ tensor T of overlap units.)
 - 2: Center overlap samples around the replica mean (dimension R).
 - 3: Pad all three spatial dimensions with $4 - [L - 1 \pmod{4}] \pmod{4}$ two-dimensional slices from each opposite end (Periodic padding ensures the input spatial length L' is $1 \pmod{4}$).
 - 4: **Convolution 1** — 16 CReLU activated channels (effectively 32 output channels). Kernel length 3. Kernel stride 2. Output spatial length $(L' - 1)/2$.
 - 5: **Convolution 2** — 64 ReLU activated channels. Kernel length 2. Dilation length 1. Output spatial length $(L' - 1)/4$.
 - 6: Reduce mean over all spatial dimensions. Output tensor size $B \times Q \times R \times 64$.
 - 7: **Fully-connected layer 1** — 32 ReLU activated units applied on the last dimension. Output tensor size $B \times Q \times R \times 32$.
 - 8: Reduce mean over the overlap sample dimension. Output tensor size $B \times Q \times 32$.
 - 9: **Fully-connected layer 2** — 3 linear units applied on the last dimension. No bias or activation. Output tensor size $B \times Q \times 3$.
 - 10: Reduce mean over the instance dimension. Output tensor size $B \times 3$.
 - 11: Softmax and inference across the batch, where 0 is the PM state, 1 is the FM state, and 2 is the SG state.
 - 12: **end procedure**
-

softmax probabilities. In every step of training, a batch of these examples of size B is evaluated into softmax probabilities, and the cost function is averaged across the batch to evaluate the gradient of the cost function.

The convolutional layers are “pool-less,” i.e., the output tensor sizes are instead controlled through the use of kernel strides and periodic padding of the overlap samples. The second convolutional kernel also has dilation, which expands the receptive field of the network [34]. The primary activation function used is the rectified linear unit (ReLU) function, which simply applies $\max(x, 0)$ on each element x of the outgoing tensor. The first convolutional layer uses the concatenated ReLU (CReLU) variant activation function, which uses twice the number of output channels as kernels to additionally utilize the negatives of learned features. This avoids the neural network having to duplicate learning effort on closely related kernels [35].

D. Monte Carlo training sets

We use parallel tempering (PT) Monte Carlo [36] to generate configurations from spin-glass instances, as well

TABLE I. Monte Carlo parameters for the instances used for training, as well as 100 instances set aside as a validation set for the confusion method. N is the number of variables, N_{sw} is the number of Monte Carlo sweeps, N_s is the number of configurations taken times independent PT runs and N_T is the number of temperatures used. EA represents the Edwards-Anderson model, FM the Ising ferromagnet.

Type	L	N	$\log_2 N_{\text{sw}}$	N_s	N_T	$[T_{\min}, T_{\max}]$
EA	8	3000	22	32×2	20	[0.20, 2.00]
EA	12	600	25	32×2	20	[0.20, 2.00]
EA	12	100	25	32×2	20	[0.20, 2.00]
FM	8	1	24	4096×4	32	[2.00, 7.00]

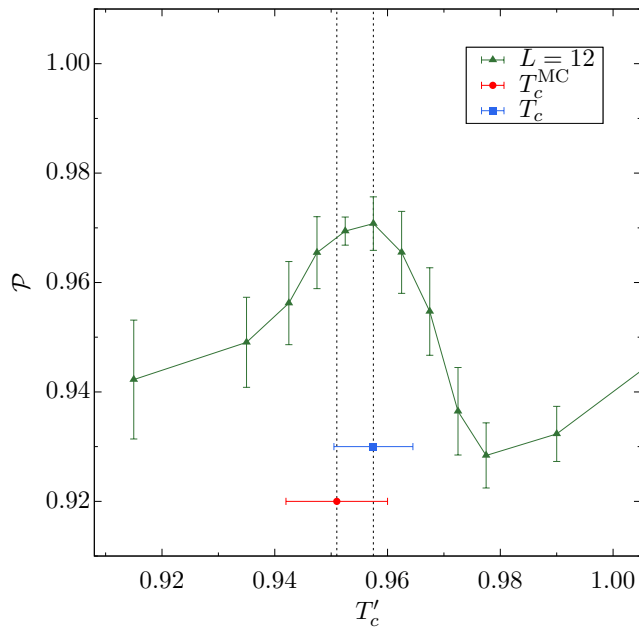


FIG. 1. Classifier accuracy as measured by Eq. (5) as the transition temperature in training is varied. An estimate of the inferred T_c (blue square) and the Monte Carlo value found in Ref. [37] (red circle) are also depicted.

as a few ferromagnet runs. Sample decorrelation is enhanced by two concurrent, independent runs of PT for each instance. Four concurrent runs are used in the case of nonzero field spin glasses.

We generate instances for the training data as outlined in Table I. The system size of $L = 8$ is small enough to thermalize easily and thus to simulate a large number of instances, yet large enough to fit with larger systems in a finite-size scaling analysis, e.g., as done in in Ref. [37]. A large amount of $L = 8$ samples can thus provide the classifier a “big picture” view of the difference between the spin-glass state and the paramagnetic state with much more uncorrelated data. A larger system size ($L = 12$) is then useful for improving the classifier’s characterization near the critical temperature. For our implementation,

TABLE II. Training parameters for the neural network. Training is divided into three stages where the parameters are adjusted for the specified amount of steps. η represents the learn rate parameter, λ the penalty weight parameter, B is the number of examples, and Q and R specify the grouping sizes for the training examples for each training step.

Steps	η	λ	B	Q	R
2000	10^{-3}	0.005	12	6	16
4000	10^{-4}	0.005	12	6	16
4000	10^{-5}	0	12	6	16

the size parameters of Algorithm 1, the learn rate parameter η , and the ℓ^2 penalty weight parameter λ , are specified in Table II. Error bars in classification probabilities and performance are derived from independently training the neural network 16 times on the training instances.

Because the classifier relies on supervised training, a critical temperature needs to be presumed before labeling the data. While this could be estimated with Monte Carlo statistics or quoted from previous results, we instead utilize the confusion method introduced in Ref. [38] to find the critical temperature. We repeat the entire training procedure for various choices of T'_c within the critical region, and select the choice that maximizes the accuracy of the classifier. We choose as our accuracy measure:

$$\mathcal{P} = \int_{T_{\min}}^{T_{\max}} dT [p_{\text{SG}}(T)\theta(T'_c - T) + p_{\text{PM}}(T)\theta(T - T'_c)], \quad (5)$$

where p_{SG} and p_{PM} are the classification probability densities of the SG and PM states between T_{\min} and T_{\max} , respectively. Naturally, because data are only collected for a discrete set of temperatures, \mathcal{P} should be calculated by a trapezoid-rule summation of the classification probabilities divided by the temperature interval measure $T_{\min} - T_{\max}$. It is important to weigh the classification probabilities as a numerical integral—and not just sum them directly—to take the uneven spacing of the simulation temperatures into account.

To simplify training, the critical temperature for classifying the FM state is simply quoted as $T_c = 4.51$ [39]. We do not attempt to optimize this transition temperature with the confusion method.

III. RESULTS

A. Confusion ensemble

The confusion method is carried out with a validation set of 100 spin-glass instances with $L = 12$, which were not used for training the classifier. The average accuracy as a function of T'_c shown in Fig. 1. The accuracy

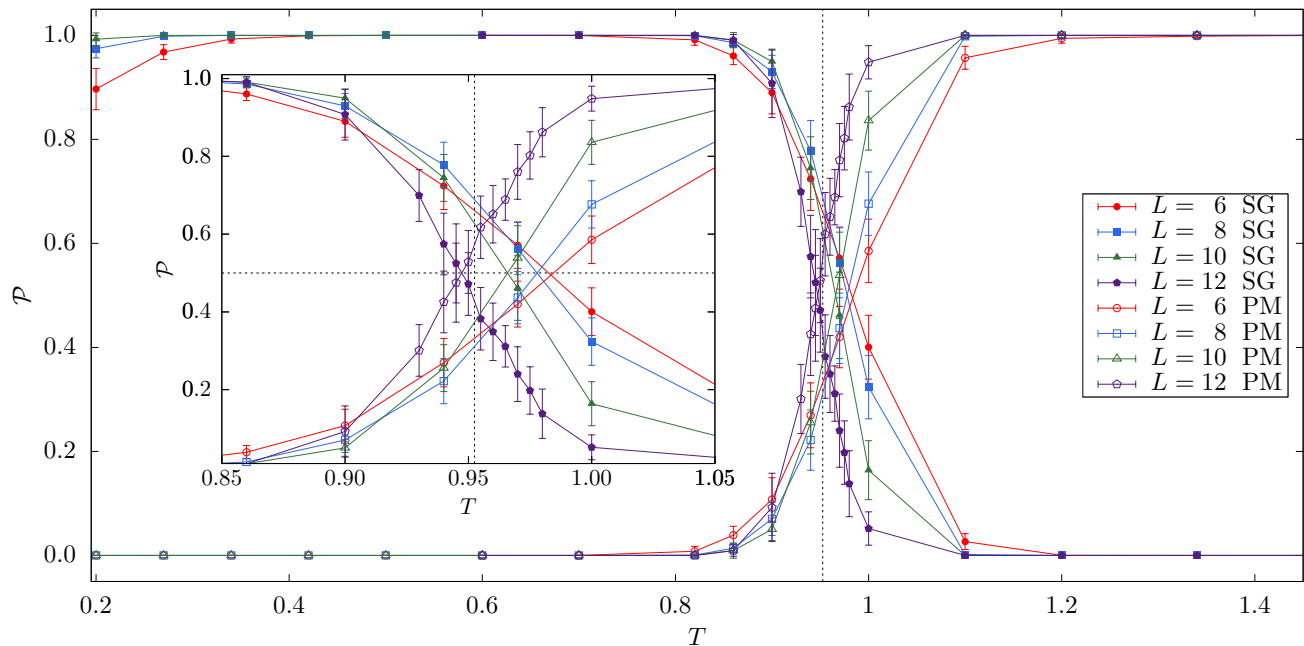


FIG. 2. Classification probabilities of the CNN for finding a spin glass (SG) or paramagnetic (PM) state. Where the probabilities do not add up to 1, the remainder belongs to FM classification probability, which is omitted for clarity. The figure inset zooms into the region between $T = 0.85$ and $T = 1.05$ where the transition in classification probability occurs for better visibility.

TABLE III. Table of parameters for each instance class simulated for a given linear size L and field strength h for the test set of examples. See Table I for additional details.

L	h	N	$\log N_{\text{sw}}$	N_s	N_T
6	0	1000	23	64	20
8	0	400	23	128	20
10	0	400	24	64	20
12	0	100	25	64	20
10	0.025	500	24	64	16
6	0.05	500	23	64	16
8	0.05	500	23	64	16
10	0.05	500	24	64	16
10	0.075	500	24	64	16
6	0.10	500	24	64	16
8	0.10	500	24	64	16
10	0.10	500	24	64	16

peak suggests a transition temperature of approximately $T_c = 0.958(8)$. This is consistent with the critical temperature of the Edwards-Anderson model with Gaussian disorder as found, for example, in Ref. [37]. The precise temperatures used as the boundary between the PM and SG states that are within the range of both T_c values are 0.953 and 0.958. In the figures that follow, we use the classifier model trained at $T'_c = 0.953$, however, the results from either model are practically identical.

The configuration samples for testing the classifier are obtained with parallel tempering Monte Carlo simulations (parameters listed in Table III).

B. Spin glasses at zero field

Figure 2 shows the classification probabilities of the classifier evaluated on the sample of spin-glass test instances. In all figures, vertical dashed lines represent transition temperatures and horizontal dashed lines the 50% probability line. The classification probabilities follow a smooth transition near the critical temperature. The classifier performs well, except for an anomalous jump in FM classification at the lowest temperature. This is likely due to the possibility of sampling instances with simple energy landscapes when dealing with finite-size spin glasses. This is supported by observing the finite size behavior as L increases to 12, for which the FM anomaly vanishes.

C. Ferromagnetic classification probabilities

Figure 3 shows the classification probabilities of the classifier on a test set of three-dimensional Ising ferromagnet samples. Note that in the CNN algorithm, the instance averaging step is kept for code consistency. An “instance” of the Ising ferromagnet is simply another set of uncorrelated configuration samples. The distinc-

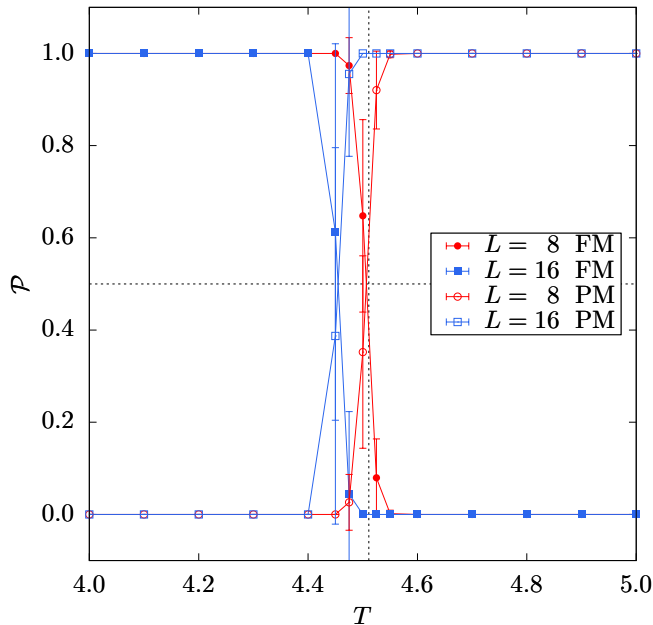


FIG. 3. Classification probabilities for the three-dimensional Ising ferromagnet. Although finite-size effects are visible, these data are only used to illustrate the detection of the FM state.

tion that the classifier learns is affected by finite-size effects, i.e., the labeling that the classifier learns for $L = 8$ ($T'_c = 4.51$) shifts for $L = 16$ ($T'_c = 4.46$) to a lower value. The classifier's sharp transition region here is likely a consequence of the number of available training parameters in the model, compared to the complexity of the learning task of distinguishing between the PM and FM states on a given system size, as well as the enhancement furnished by averaging over multiple configuration samples.

In principle, the characteristics of these classification probabilities may be useful as a NN-based finite-size scaling technique. However, neither learning the three-dimensional Ising ferromagnetic transition temperature to high precision nor inferring its critical properties from the NN were initial objectives in this work.

D. Generalization to bimodal disorder

As a first generalization test, we generate a test set of spin-glass instances with bimodal instead of Gaussian disorder. In this case, the critical temperature shifts to $T_c \approx 1.12$ [37]. The crossover point easily shifts to this new temperature. We take this as very good evidence that the classifier learns a good representation of the spin-glass state, and can make accurate predictions for different spin-glass models with different disorder distributions.

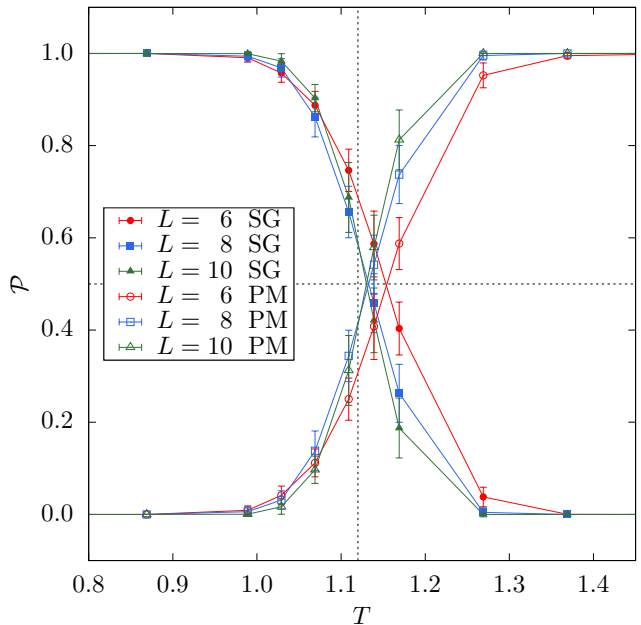


FIG. 4. Classification probabilities of CNN trained on the Edwards-Anderson spin glass with Gaussian disorder with a test set of instances with bimodal disorder. The data cross close to $T'_c \approx 1.1$, the known value of the bimodal spin-glass transition temperature.

E. Generalization to nonzero fields

Now that we have demonstrated that our NN can detect a spin-glass transition at zero field and even detect correct transition temperatures when the disorder is changed, we analyze the existence of a spin-glass state in a field. The classification probabilities for nonzero fields are shown in Figure 5. It can be observed that even at $h = 0.05$, the spin-glass signal for the classifier becomes weak. At a stronger field, $h = 0.10$, the PM phase is clearly dominant with larger linear system sizes L . Figure 6 clearly illustrates a break down of any crossing temperature beyond system sizes of $L = 6$.

A possible objection could be that, for $L = 10$, there appears to be a region between $h = 0.0$ and $h = 0.05$ where the classification probability is significant. Could a transition simply be somewhere there? As was pointed out, e.g., in Ref. [17], fields of strength $h \approx 0.1$ are far below the predicted critical field from mean-field calculations, namely $h_{AT} \approx 0.65$. The results presented here thus suggest that if there is a spin-glass state in a field, it must occur for fields $h \lesssim 0.05$.

IV. SUMMARY AND CONCLUSION

We have implemented and evaluated an input-size agnostic three-dimensional convolutional neural network for ternary phase classification on Ising-like models three-

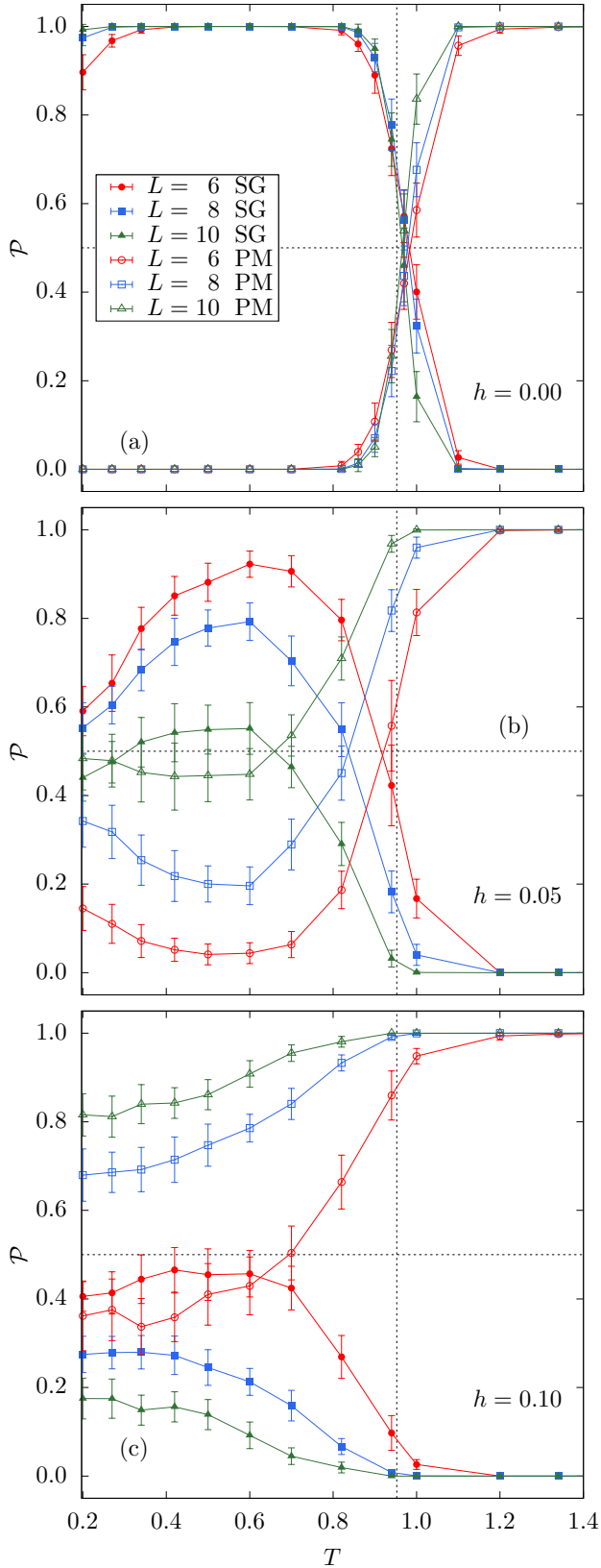


FIG. 5. Progression of classification probabilities for different fields. As the field increases, the SG signal weakens progressively. Even for fields as weak as $h = 0.05$ the signal of the transition moves to zero temperature as the system size increases. Data for (a) $h = 0.00$, (b) $h = 0.05$, and (c) $h = 0.10$.

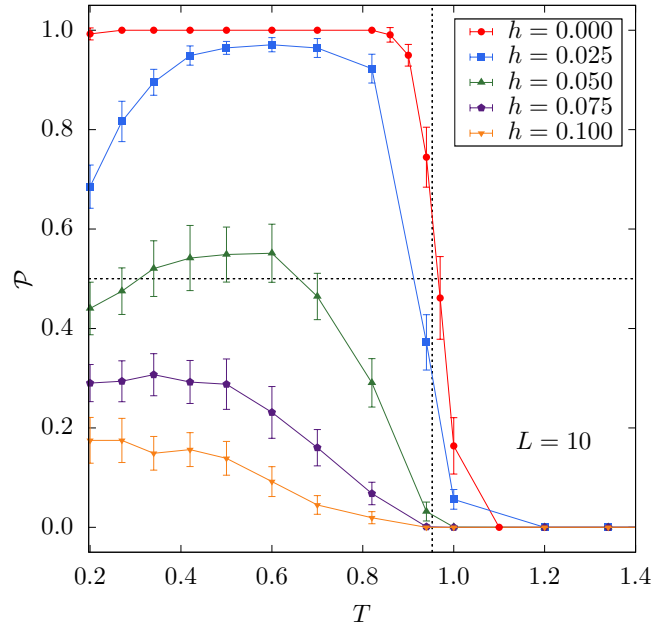


FIG. 6. Progression of classification probabilities with increasing system size for $L = 10$. The stronger the field, the weaker the signal for a SG state.

dimensional cubic lattice and find strong evidence of learning an accurate representation of the spin-glass state. We emphasize that this is nontrivial, because of the lack of spatial order in these systems. Furthermore, the approach can be generalized to other three-dimensional models.

In general, NNs once optimized could be used to probe the phase characteristics of modified spin-glass models where Monte Carlo statistics may happen to be unavailable or inconclusive. Examples are systems where no local order parameter exists, such as in lattice gauge theories found for some error models when determining error thresholds for topological codes [40–45].

Similarly, we demonstrate without the use of the standard order parameters that a spin-glass state in a field might not be stable for three-dimensional systems. It is important to emphasize that the numerical effort needed is considerably smaller in this case: Whereas most spin-glass studies require tens of thousands of samples, in this work conclusions can be drawn from as little as 500 disorder instances.

Further computational and theoretical research in this disciplinary interface may be encouraging. Both neural networks and spin glasses are examples of complex systems with a breadth of applications, where in fact some neural networks can find a description though long-range spin glasses [46]. The converse study of describing spin glasses through neural networks may prove rewarding from the point of view of complexity theory.

V. ACKNOWLEDGMENTS

We would like to thank Amin Barzegar, Chao Fang and Evert van Nieuwenburg for comments and useful discussions. H. M. B. acknowledges financial support from the Marianne '76 and Robert '77 Hamm Endowed Scholarship from the Department of Physics and Astronomy while a student at Texas A&M University. The research of H. M. B. is based upon work (partially) supported by the Office of the Director of National Intelligence (ODNI), Intelligence Advanced Research Projects Activity (IARPA), via the U.S. Army Research Office contract W911NF-17-C-0050. H. G. K. acknowledge support from the National Science Foundation (Grant No. DMR-

1151387). The work of H. G. K. is supported in part by the Office of the Director of National Intelligence (ODNI), Intelligence Advanced Research Projects Activity (IARPA), via MIT Lincoln Laboratory Air Force Contract No. FA8721-05-C-0002. The views and conclusions contained herein are those of the authors and should not be interpreted as necessarily representing the official policies or endorsements, either expressed or implied, of ODNI, IARPA, or the U.S. Government. The U.S. Government is authorized to reproduce and distribute reprints for Governmental purpose notwithstanding any copyright annotation thereon. We thank Texas A&M University for access to their Ada and Terra clusters.

-
- [1] S. O. Haykin, *Neural Networks and Learning Machines* (Pearson, 2008).
- [2] I. Goodfellow, Y. Bengio, and A. Courville, *Deep Learning* (MIT Press, 2016), <http://www.deeplearningbook.org>.
- [3] C. Bishop, *Pattern Recognition and Machine Learning* (Springer-Verlag, New York, 2006).
- [4] J. Carrasquilla and R. G. Melko, *Machine learning phases of matter*, *Nature Physics* **13**, 431 (2017).
- [5] K. Ch'ng, J. Carrasquilla, R. G. Melko, and E. Khatami, *Machine Learning Phases of Strongly Correlated Fermions*, *Phys. Rev. X* **7**, 031038 (2017).
- [6] K. Binder and A. P. Young, *Spin Glasses: Experimental Facts, Theoretical Concepts and Open Questions*, *Rev. Mod. Phys.* **58**, 801 (1986).
- [7] M. Mézard, G. Parisi, and M. A. Virasoro, *Spin Glass Theory and Beyond* (World Scientific, Singapore, 1987).
- [8] A. P. Young, ed., *Spin Glasses and Random Fields* (World Scientific, Singapore, 1998).
- [9] D. L. Stein and C. M. Newman, *Spin Glasses and Complexity*, *Primers in Complex Systems* (Princeton University Press, Princeton NJ, 2013).
- [10] G. Parisi, *The order parameter for spin glasses: a function on the interval 0–1*, *J. Phys. A* **13**, 1101 (1980).
- [11] D. S. Fisher and D. A. Huse, *Ordered phase of short-range Ising spin-glasses*, *Phys. Rev. Lett.* **56**, 1601 (1986).
- [12] D. S. Fisher and D. A. Huse, *Equilibrium behavior of the spin-glass ordered phase*, *Phys. Rev. B* **38**, 386 (1988).
- [13] M. A. Moore and A. J. Bray, *Disappearance of the de Almeida-Thouless line in six dimensions*, *Phys. Rev. B* **83**, 224408 (2011).
- [14] M. A. Moore, *1/m expansion in spin glasses and the de Almeida-Thouless line*, *Phys. Rev. E* **86**, 031114 (2012).
- [15] S. Caracciolo, G. Parisi, S. Patarnello, and N. Sourlas, *3d Ising spin-glasses in a magnetic field and mean-field theory*, *Europhys. Lett.* **11**, 783 (1990).
- [16] J. Houdayer and O. C. Martin, *Ising spin glasses in a magnetic field*, *Phys. Rev. Lett.* **82**, 4934 (1999).
- [17] A. P. Young and H. G. Katzgraber, *Absence of an Almeida-Thouless line in Three-Dimensional Spin Glasses*, *Phys. Rev. Lett.* **93**, 207203 (2004).
- [18] H. G. Katzgraber and A. P. Young, *Probing the Almeida-Thouless line away from the mean-field model*, *Phys. Rev. B* **72**, 184416 (2005).
- [19] M. Sasaki, K. Hukushima, H. Yoshino, and H. Takayama, *Scaling Analysis of Domain-Wall Free Energy in the Edwards-Anderson Ising Spin Glass in a Magnetic Field*, *Phys. Rev. Lett.* **99**, 137202 (2007).
- [20] T. Jörg, H. G. Katzgraber, and F. Krzakala, *Behavior of Ising Spin Glasses in a Magnetic Field*, *Phys. Rev. Lett.* **100**, 197202 (2008).
- [21] H. G. Katzgraber, D. Larson, and A. P. Young, *Study of the de Almeida-Thouless line using power-law diluted one-dimensional Ising spin glasses*, *Phys. Rev. Lett.* **102**, 177205 (2009).
- [22] D. Larson, H. G. Katzgraber, M. A. Moore, and A. P. Young, *Spin glasses in a field: Three and four dimensions as seen from one space dimension*, *Phys. Rev. B* **87**, 024414 (2013).
- [23] E. Marinari, G. Parisi, and J. Zuliani, *Four-dimensional spin glasses in a magnetic field have a mean-field-like phase*, *J. Phys. A* **31**, 1181 (1998).
- [24] L. Leuzzi, G. Parisi, F. Ricci-Tersenghi, and J. J. Ruiz-Lorenzo, *Ising Spin-Glass Transition in a Magnetic Field Outside the Limit of Validity of Mean-Field Theory*, *Phys. Rev. Lett.* **103**, 267201 (2009).
- [25] J. F. Fernández, *Evidence against an Almeida-Thouless line in disordered systems of Ising dipoles*, *Phys. Rev. B* **82**, 144436 (2010).
- [26] M. Baity-Jesi, R. Alvarez Baños, A. Cruz, L. A. Fernandez, J. M. Gil-Narvon, Gordillo-Guerrero, D. Iñiguez, A. Maiorano, F. Mantovani, E. Marinari, et al., *Dynamical transition in the $D = 3$ Edwards-Anderson spin glass in an external magnetic field*, *Phys. Rev. E* **89**, 032140 (2014).
- [27] M. C. Angelini and G. Biroli, *Spin Glass in a Field: A New Zero-Temperature Fixed Point in Finite Dimensions*, *Phys. Rev. Lett.* **114**, 095701 (2015).
- [28] J. R. L. de Almeida and D. J. Thouless, *Stability of the Sherrington-Kirkpatrick solution of a spin glass model*, *J. Phys. A* **11**, 983 (1978).
- [29] C. M. Newman and D. L. Stein, *Short-range spin glasses: Results and speculations*, in *Lecture Notes in Mathematics 1900* (Springer-Verlag, Berlin, 2007), p. 159, (condmat/0503345).
- [30] M. Abadi et al., *TensorFlow: A System for Large-Scale Machine Learning* (2016), <http://tensorflow.org>.

- [31] S. F. Edwards and P. W. Anderson, *Theory of spin glasses*, J. Phys. F: Met. Phys. **5**, 965 (1975).
- [32] J. M. Yeomans, *Statistical Mechanics of Phase Transitions* (Oxford University Press, Oxford, 1992).
- [33] D. P. Kingma and J. Ba, *Adam: A Method for Stochastic Optimization* (2014), (arXiv:1412.6980).
- [34] F. Yu and V. Koltun, *Multi-scale context aggregation by dilated convolutions* (2015).
- [35] W. Shang, K. Sohn, D. Almeida, and H. Lee, *Understanding and Improving Convolutional Neural Networks via Concatenated Rectified Linear Units*, International Conference on Machine Learning p. 2217 (2016), (arXiv:1603.05201).
- [36] K. Hukushima and K. Nemoto, *Exchange Monte Carlo method and application to spin glass simulations*, J. Phys. Soc. Jpn. **65**, 1604 (1996).
- [37] H. G. Katzgraber, M. Körner, and A. P. Young, *Universality in three-dimensional Ising spin glasses: A Monte Carlo study*, Phys. Rev. B **73**, 224432 (2006).
- [38] E. P. L. van Nieuwenburg, Y.-H. Liu, and S. D. Huber, *Learning phase transitions by confusion*, Nat. Phys. **13**, 435 (2017).
- [39] K. Binder and E. Luijten, *Monte carlo tests of renormalization-group predictions for critical phenomena in ising models*, Phys. Rep **344**, 179 (2001).
- [40] E. Dennis, A. Kitaev, A. Landahl, and J. Preskill, *Topological quantum memory*, J. Math. Phys. **43**, 4452 (2002).
- [41] G. Arakawa, I. Ichinose, T. Matsui, and K. Takeda, *Self-duality and phase structure of the 4D random-plaquette Z_2 gauge model*, Nucl. Phys. B **709**, 296 (2005).
- [42] H. G. Katzgraber, H. Bombin, and M. A. Martin-Delgado, *Error Threshold for Color Codes and Random 3-Body Ising Models*, Phys. Rev. Lett. **103**, 090501 (2009).
- [43] R. S. Andrist, H. G. Katzgraber, H. Bombin, and M. A. Martin-Delgado, *Tricolored Lattice Gauge Theory with Randomness: Fault-Tolerance in Topological Color Codes*, New J. Phys. **13**, 083006 (2011).
- [44] H. Bombin, R. S. Andrist, M. Ohzeki, H. G. Katzgraber, and M. A. Martin-Delgado, *Strong Resilience of Topological Codes to Depolarization*, Phys. Rev. X **2**, 021004 (2012).
- [45] R. S. Andrist, H. Bombin, H. G. Katzgraber, and M. A. Martin-Delgado, *Optimal error correction in topological subsystem codes*, Phys. Rev. A **85**, 050302 (2012).
- [46] H. Nishimori, *Statistical Physics of Spin Glasses and Information Processing: An Introduction* (Oxford University Press, New York, 2001).